ACS APPLIED MATERIALS & INTERFACES

www.acsami.org

Research Article

Guided Electrokinetic Assembly of Polystyrene Microbeads onto Photopatterned Carbon Electrode Arrays

Tuo Zhou, Jingyuan Chen, Ethan Kropp, and Lawrence Kulinsky*

Cite This: https://dx.doi.org/10.1021/acsami.0c08266

Read Online

ACCESS | Metrics & More | Article Recommendations | Supporting Information

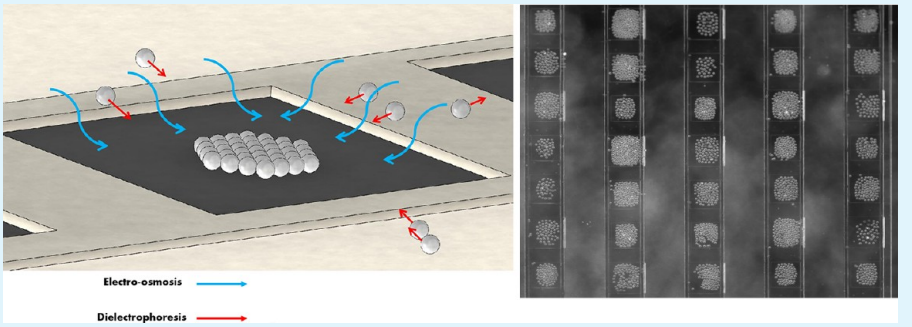

ABSTRACT: Assembly of microdevices from constituent parts currently relies on slow serial steps via direct assembly processes such as pick-and-place operations. Template Electrokinetic Assembly (TEA), a guided, noncontact assembly process, is presented in this work as a promising alternative to serial assembly processes. To characterize the process and its implementation of electrokinetic, dielectrophoretic, and electro-osmotic phenomena, we conducted studies to examine the assembly of polymer microparticles at specific locations on glassy carbon interdigitated electrode arrays (IDEAs). The IDEAs are coated with a layer of lithographically patterned resist, so that when an AC electric field is applied to the IDEA, microparticles suspended in the aqueous solution are attracted to the open regions of the electrodes not covered by photoresist. Interplay between AC electro-osmosis and dielectrophoretic forces guides 1 and 5 μm diameter polystyrene beads to assemble in regions, or "wells", uncovered by photoresist atop the electrodes. It was discovered that AC electro-osmosis under an applied frequency of 1 kHz is sufficient to effectively agglomerate 1 μm beads in the wells, whereas a stepwise process involving the application of a 1 MHz signal, followed by a 1 kHz signal, is required for the positioning of 5 μm beads, which are mainly affected by dielectrophoretic forces. Permanent entrapment of the microparticles is then demonstrated via the electropolymerization process of the conducting polymer polypyrrole.

KEYWORDS: *microassembly, electrokinetics, dielectrophoresis, electro-osmosis, lithography*

1. INTRODUCTION

Fabrication of microdevices is often limited by the speed, cost, and precision of assembling individual components onto predetermined locations.[1] Among available microassembly techniques, direct-assembly (also called pick-and-place) and self-assembly play prominent roles.[2,3] However, these assembly techniques have significant drawbacks.

Self-assembly refers to the spontaneous assembly and organization of small parts into patterns at the nano- and microscale without direct outside intervention.[3,4] Yet because self-assembly is designed to operate on a molecular level, it is not suitable for microparts and furthermore cannot be used to direct microscopic and mesoscopic parts to specified locations.[4] Pick-and-place techniques move individual parts either through a contact force (such as with microgrippers or tweezers), or through a noncontact force (for example, using optical tweezers).[5−7] While positioning with pick-and-place techniques can be fairly accurate, its operation can suffer from reliability of part release because of surface adhesion, surface tension, and electrostatic forces.[8−10] Additionally, pick-and-place systems often rely on expensive robotic systems, and the serial nature of the process means that such an approach requires a long time to assemble a microsystem consisting of many small parts.[11,12] Finally, the manipulators incorporated in these robotic systems are typically quite large, limiting the portability and miniaturization prospects for such pick-and-place assembly platforms.[6]

Guided electrokinetic assembly, which utilizes dielectrophoresis (DEP) and electro-osmosis (EO), combines positive characteristics of both self- and direct-assembly techniques.[13] Guided electrokinetic assembly techniques operate on the

Received: May 7, 2020
Accepted: July 9, 2020

proper scale for the assembly of microparts and implement a noncontact approach to positioning parts, which enables a fast throughput originally characteristic of self-assembly techniques. Furthermore, both DEP and EO have found widespread utilization in the transportation, separation, sorting, and assembly of nano- and microparticles and cells.[14−24] However, often because of the presence of forces that are difficult to measure and control (e.g., thermal forces, viscous forces in the fluid, particle-to-particle interactions, etc.), particle placement using electrokinetic forces is less accurate than part placement performed with many pick-and-place systems.[25]

In this article, we report a novel guided microassembly technique that possesses the speed of self-assembly techniques while still maintaining the precision of direct-assembly techniques. This new technique utilizes a combination of guided dielectrophoresis (DEP) and AC electro-osmosis (ACEO) in conjunction with glassy carbon interdigitated electrode arrays (IDEAs). The IDEAs are further patterned with a layer of photoresist to define "windows", or exposed regions where microparticulates are to be positioned. In this study, polymer microbeads are suspended in deionized (DI) water and are guided by ACEO and DEP to assemble within the wells on top of the microelectrodes. Once microparts are attracted into their predetermined locations on the electrodes, they are permanently attached via the electropolymerization of a thin layer of the conducting polymer polypyrrole (PPy).[26−28] Because the discussed guided assembly process is not serial in nature, it can be scaled up to achieve simultaneous assembly of a great number of micro- and nanoparts.

AC electro-osmosis describes the nonlinear flow around a polarized surface, caused by interactions between an external AC electric field and ionic charges accumulated in the diffuse double layer on an electrode surface.[29] AC electro-osmosis generated with coplanar bar electrodes has been studied extensively.[30,31] For ACEO, the velocity of the flow is primarily dependent on both the applied frequency and the magnitude of the field's strength.[32] The velocity of the flow is negligible at extremely low frequencies and gradually grows with increasing frequency.[31] As frequency is increased, the velocity of the flow has the propensity to increase sharply until a maximum flow is reached, marked by some critical frequency (generally below 10 kHz). From this critical frequency, the velocity of the flow continues to decrease with increasing frequency until another minimum is reached. Generally, for cases in which the double layer is thin, in quasi-equilibrium (where ω is comparable to (σ/ε)), and on a perfectly polarizable metal electrode, the velocity of the flow can be quantitatively analyzed with the Helmholtz−Smoluchowski equation:[33]

$$u = -\frac{\varepsilon}{\eta}\Delta\phi_{\mathrm{d}}\frac{\partial\phi}{\partial x} \tag{1}$$

where u is the velocity of the fluid, ε is the permittivity of the fluid, η the viscosity of the fluid, ϕ is the potential of the field outside the diffuse double layer, and $\Delta\phi_{\mathrm{d}}$ is the difference in potential between the outer and inner portions of the diffuse double layer.

Dielectrophoresis refers to the force exerted by a nonuniform external electric field on the induced dipole moment of a dielectric particle, suspended in a dielectric medium.[34] The frequency of the applied AC field affects both the complex permittivities of the particle and fluid medium. This variance in the complex permittivities between the particle and medium throughout a range of frequencies affects the value and sign of the real part of the Clausius−Mossotti factor (CM) and thus influences the direction and affects the magnitude of the DEP force. The DEP force is shown below in eq 2:[35]

$$\langle F_{\mathrm{DEP}}\rangle = 2\pi r^3\varepsilon_{\mathrm{m}}Re\{CM(\omega)\}\nabla|E|^2 \tag{2}$$

$$CM = \left\{\frac{\varepsilon_{\mathrm{p}}^* - \varepsilon_{\mathrm{m}}^*}{\varepsilon_{\mathrm{p}}^* + 2\varepsilon_{\mathrm{m}}^*}\right\} \tag{3}$$

$$\varepsilon^* = \varepsilon_{\mathrm{r}} + i\frac{\sigma}{\omega} \tag{4}$$

where $\nabla|E|^2$ represents the gradient of the electric field magnitude squared, r the radius of the particle, ε_{m} the relative permittivity of the medium, and $\varepsilon_{\mathrm{m}}^*$ and $\varepsilon_{\mathrm{p}}^*$ are the complex permittivities of the fluid medium and particle, respectively. In general, if the real part of the complex permittivity of the particle is greater than that of the fluid medium, the DEP force will be "positive", or in the direction of the field's intensity gradient, causing the particles to travel toward the electrodes. However, if the real part of the complex permittivity of the particle is smaller than the fluid medium, the particle will experience a "negative" DEP force (nDEP), and will travel opposite the intensity gradient and toward regions of lower field magnitude, moving away from the electrode edges.

The guided electrokinetic assembly of microparticles based on photopatterned insulating templates is described and discussed here for the first time. Although polymer microbeads are used in the discussion of the assembly process, the use of such templates can be extended to the assembly of parts or particles of various materials such as metals, organic, and nonorganic matter, and may be employed for nanoparticles as well. Therefore, this guided electrokinetic template-based assembly process has a wide range of possible applications, from the creation of a surface enhanced Raman spectroscopy (SERS) array, to the fabrication of biochips with deposited and entrapped cells.[36,37]

2. EXPERIMENTAL SECTION

The glassy carbon IDEAs used in the experiments were fabricated through conventional lithography techniques from SU-8 photoresist and were subsequently pyrolyzed[38] to convert the organic resist into carbon. The IDEAs were fabricated on 4 in. diameter silicon wafers covered with a 1 μm thick layer of thermal oxide (University Wafer, MA, USA). SU-8 2025 photoresist (Microchem Corp. Ltd., MA, USA) was spin-coated onto the wafer at an initial speed of 500 rpm for 10 s, followed by an increase in the angular velocity of the spinner to 4000 rpm for 30 s using a Laurell photoresist spinner (Laurell Technologies, PA, USA). Following the spin cycle, the wafer was soft baked to 95 °C for 5 min on a Dataplate Pmc 732 hot plate (Dataplate Pmc 732 Series, IA, USA). Next, the wafer was exposed through a plastic mask (CadArt, OR, USA) to UV light with a UV flood exposure system (Oriel Instrument, Newport Corp, CA, USA) for 6 s at an energy intensity of 10 mW/cm^2 to create the IDEA pattern. The wafer was postbaked on the hot plate at 65 °C for 1 min, and then at 95 °C for 5 min. SU-8 developer (Microchem Corp. Ltd., MA, USA) was utilized to etch out the uncross-linked regions of the photoresist. The wafer was then hard baked at 95 °C for 45 min. Lastly, the IDEA was carbonized inside a furnace (Thermo Fisher Scientific, Thermo Scientific, MA, USA), using the thermal profile presented in Figure S1a. After the pyrolysis process, the heights of the glassy carbon IDEA fingers were measured with a Dektak 3 profilometer (Veeco Instrument Inc., NY, USA) and found to be between 1.5 and 2.0 μm in height and 120−126 μm in width.

A layer of SU-8 photoresist was then coated over the IDEAs and lithographically patterned to form an array of wells in the resist layer. Figure 1a−c presents the schematics and the optical micrograph of the

https://dx.doi.org/10.1021/acsami.0c08266
ACS Appl. Mater. Interfaces XXXX, XXX, XXX−XXX

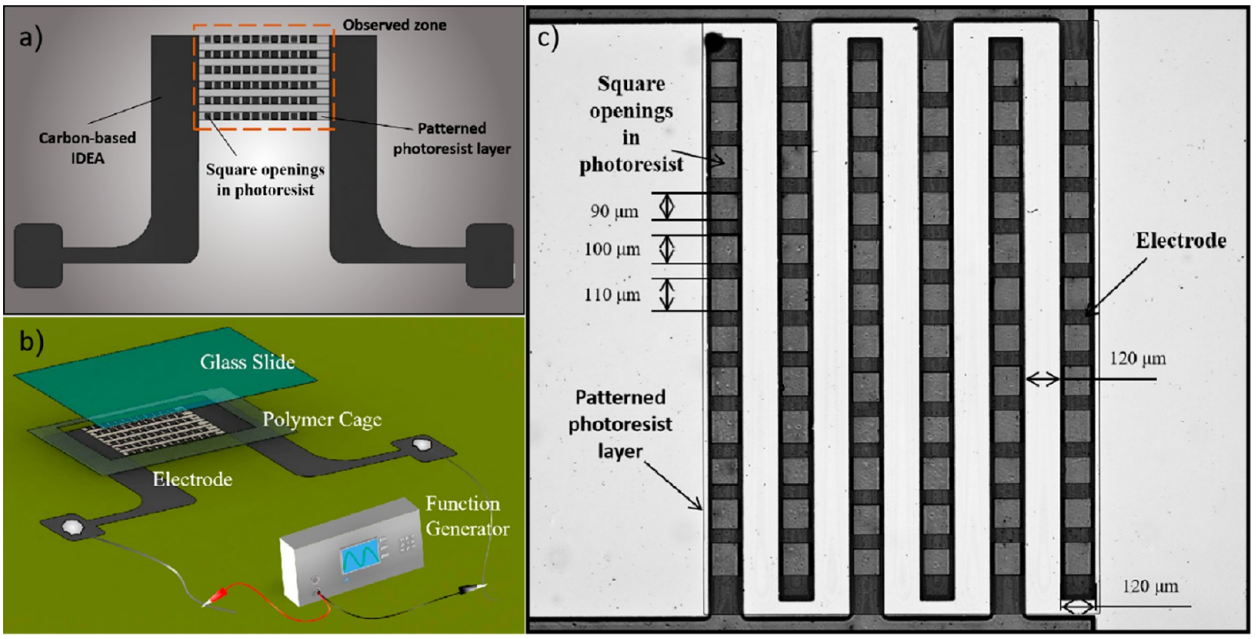

Figure 1. (a) Schematics of the IDEA chip with polymer cage created from double-stick tape and covered by the glass slide; (b) sketch of the interdigitated electrode arrays; (c) optical micrograph of the electrode fingers covered with square wells opened in the photoresist.

IDEAs where each 120 μm wide electrode finger is separated by a 120 μm gap between the adjacent fingers. The design of the patterned photoresist layer consists of an array of alternating well sizes (90 × 90 μm, 100 × 100 μm,110 × 110 μm). These wells were produced via conventional lithography techniques utilizing an iron oxide mask (Front Range Photomask, AZ, USA) and a MA 56 mask aligner (Karl Suss, Germany). The thin layer of SU-8 2002 photoresist was spin-coated on the surface of the IDEA, and the subsequent soft-bake, exposure, and postexposure bake processes were all adjusted depending on the desired height of the resist layer. For a photoresist layer height of 3 μm, the resist was soft baked for 2 min at 95 °C, exposed for 4 s at an energy intensity of 10 mW/cm2 using the MA56 mask aligner's embedded light source, and postbaked for 3 min. The wafer was then hard baked at 95 °C for 45 min. For a resist height of 6 μm, the photoresist was soft baked for 3 min at 95 °C and exposed for 6 s with the same masker aligner and light source as before. The second layer was then postbaked for 5 min at 95 °C. Afterward, the un-cross-linked regions of the photoresist were etched away using the same SU-8 developer for 5 min. Lastly, the second layer was hard baked at 95 °C for 45 min.

Aqueous solutions of 1 and 5 μm diameter carboxyl-modified latex (CML) polystyrene beads (Thermal Fisher Scientific, Invitrogen, MA, USA), both possessing a weight percent of 4 wt % in their original media, were segregated and diluted to a new concentration of 0.39 wt % in DI water by placing the original solutions in a centrifuge (Eppendorf, Germany) for 10 min at 1500 rpm. The supernatant was removed with a pipet and the beads were mixed with the appropriate amount of DI water to achieve a 0.39 wt % solution.

After the IDEAs were fabricated, wires were soldered to the carbon contact pads of the IDEA chips using indium, and double-stick tape (3M, MN, USA) was cut to construct the fluidic chamber around the electrodes as presented in Figure 1a. A 20 μL droplet was pipetted on top of the electrodes, and a glass cover slide (Thermal Fisher Scientific, Fisherbrand, MA, USA) was placed over the chip to facilitate microscopic observation and reduce evaporation of the fluid. A Nikon eclipse microscope (Nikon, Japan) and SPOT Basic video editing program (SPOT Imaging, MI, USA) were used to observe and record the motion of the particles. The IDEA chip was connected to a function generator (Stanford Research System, CA, USA) to produce the AC field with any desired frequency and peak-to-peak voltage. Photos of the IDEA chip and lab setup are presented in Figures S1b, c.

After the beads are attracted in the designated locations, they can be permanently entrapped via electropolymerization in the mixed solution of 0.1 M pyrrole monomers and 0.1 M NaDBS (sodium dodecylbenzene-sulfonate). The 100 μL polymerization solution is mixed with 1 mL of the bead suspension, and placed in an ultrasonic vibrator (Emersion Electric Co., MO, USA) for 30 min to prevent the colloid from flocculating. For each trial, 20 μL of the mixture was deposited onto the fingers of the electrodes and a glass lid was placed to cover the solution and IDEA. The electrodeposition of polypyrrole from the mixture was initiated by applying a 0.9 V DC offset for 60 s after the microbeads were positioned inside the wells after the guided assembly process.

3. RESULTS AND DISCUSSION

3.1. Steps of Template Electrokinetic Assembly. The goal of the template electrokinetic assembly (TEA) process under study is to collect 1 and 5 μm polystyrene microbeads into specific locations where the carbon electrodes are exposed. These locations, or "wells," are shown in Figure 1a–c. Within the positive DEP regime, such as at an applied frequency of 1 kHz, 1 μm beads immediately gathered inside the wells (as seen in Movies S1 and S2 and captured in the time-lapse images shown in Figure 2 below). However, when the same frequency was used for the 5 μm bead suspension, most of the microbeads did not travel toward the wells. This can be explained by the fact that the viscous drag for the 5 μm beads is significantly greater than that for the 1 μm beads. The influence of particle size is demonstrated with Stokes law (eq 5), which describes the viscous drag, F_d, that is experienced by a spherical particle of radius R moving through a fluid medium:[39]

$$F_d = 6\pi\mu R\upsilon \tag{5}$$

where μ is the dynamic viscosity of the media and υ is the velocity of the particle with respect to the media.

Because the larger drag forces experienced by the 5 μm beads prevent them from being positioned inside the wells upon initial application of a pDEP force, a two-step process incorporating both pDEP, nDEP, and EO flow is needed. For the first step, nDEP is applied to the beads using an AC field of 1 MHz applied

https://dx.doi.org/10.1021/acsami.0c08266
ACS Appl. Mater. Interfaces XXXX, XXX, XXX−XXX

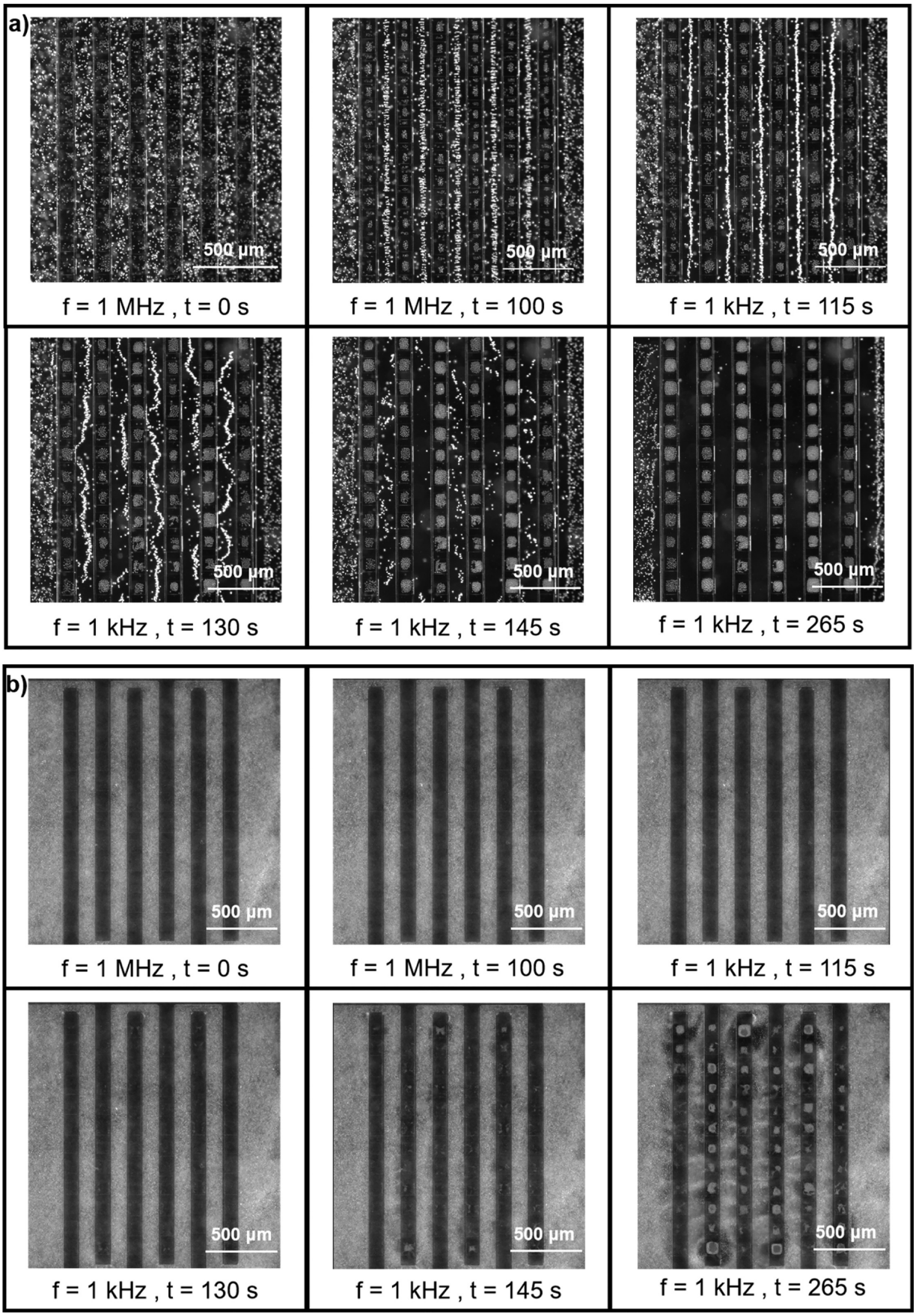

Figure 2. Process of template electrokinetic assembly (TEA) of (a) 5 μm and (b) 1 μm polystyrene microbeads.

https://dx.doi.org/10.1021/acsami.0c08266
ACS Appl. Mater. Interfaces XXXX, XXX, XXX−XXX

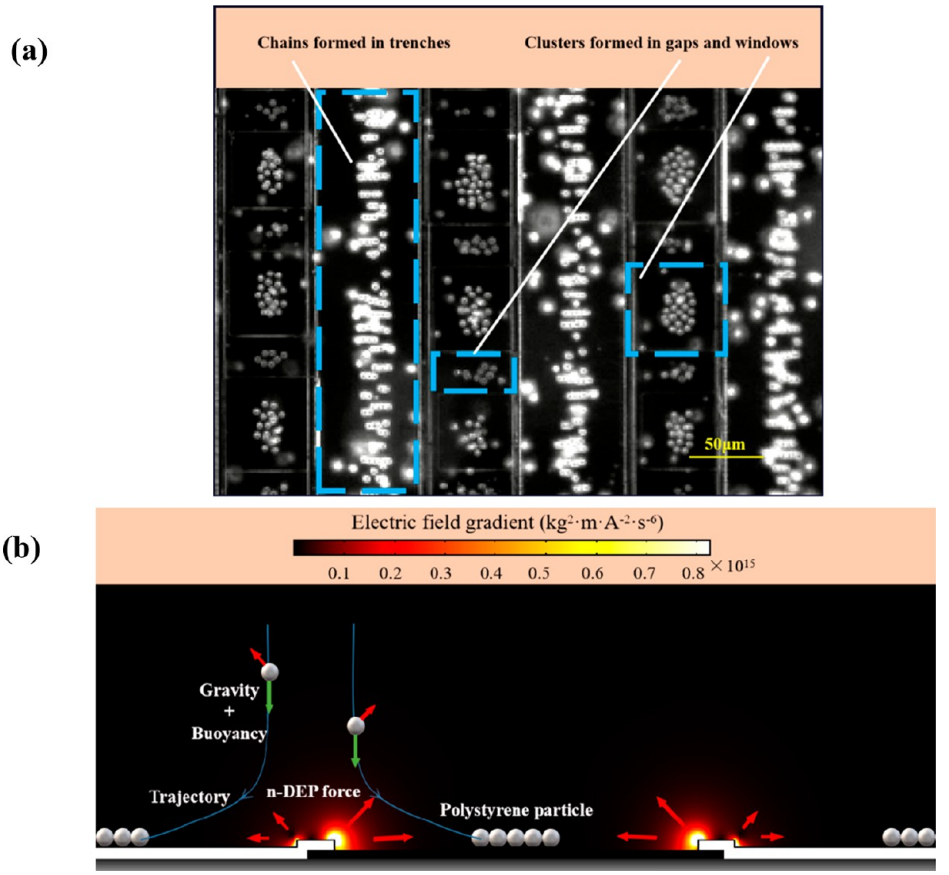

Figure 3. (a) Patterns formed by 5 μm particles under the effect of nDEP under 1 MHz, 4 Vpp AC bias; (b) COMSOL simulation results reflect the combination of gravitational sedimentation and nDEP on polystyrene beads and explains the formation of the observed initial bead pattern.

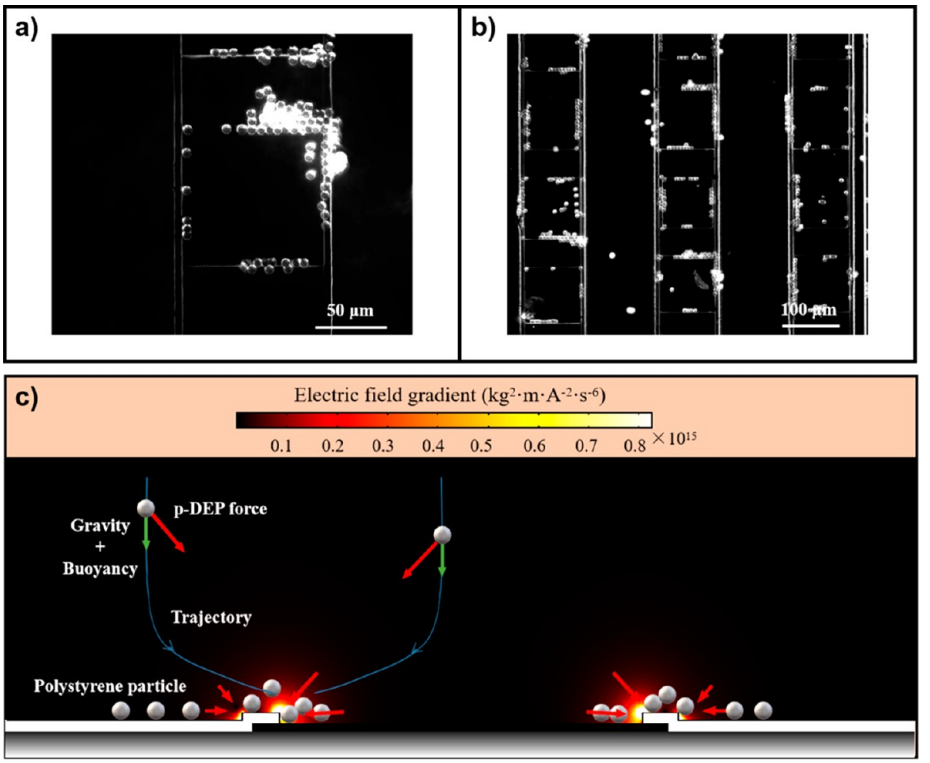

Figure 4. (a, b) Positive iDEP from the edges of the wells attracts 5 μm polystyrene beads at 1 kHz and 3 Vpp as demonstrated by the optical micrographs. (c) Results of COMSOL simulation demonstrate that under positive DEP the beads will move toward the photoresist edges around the windows that have the highest electric field gradient.

https://dx.doi.org/10.1021/acsami.0c08266
ACS Appl. Mater. Interfaces XXXX, XXX, XXX−XXX

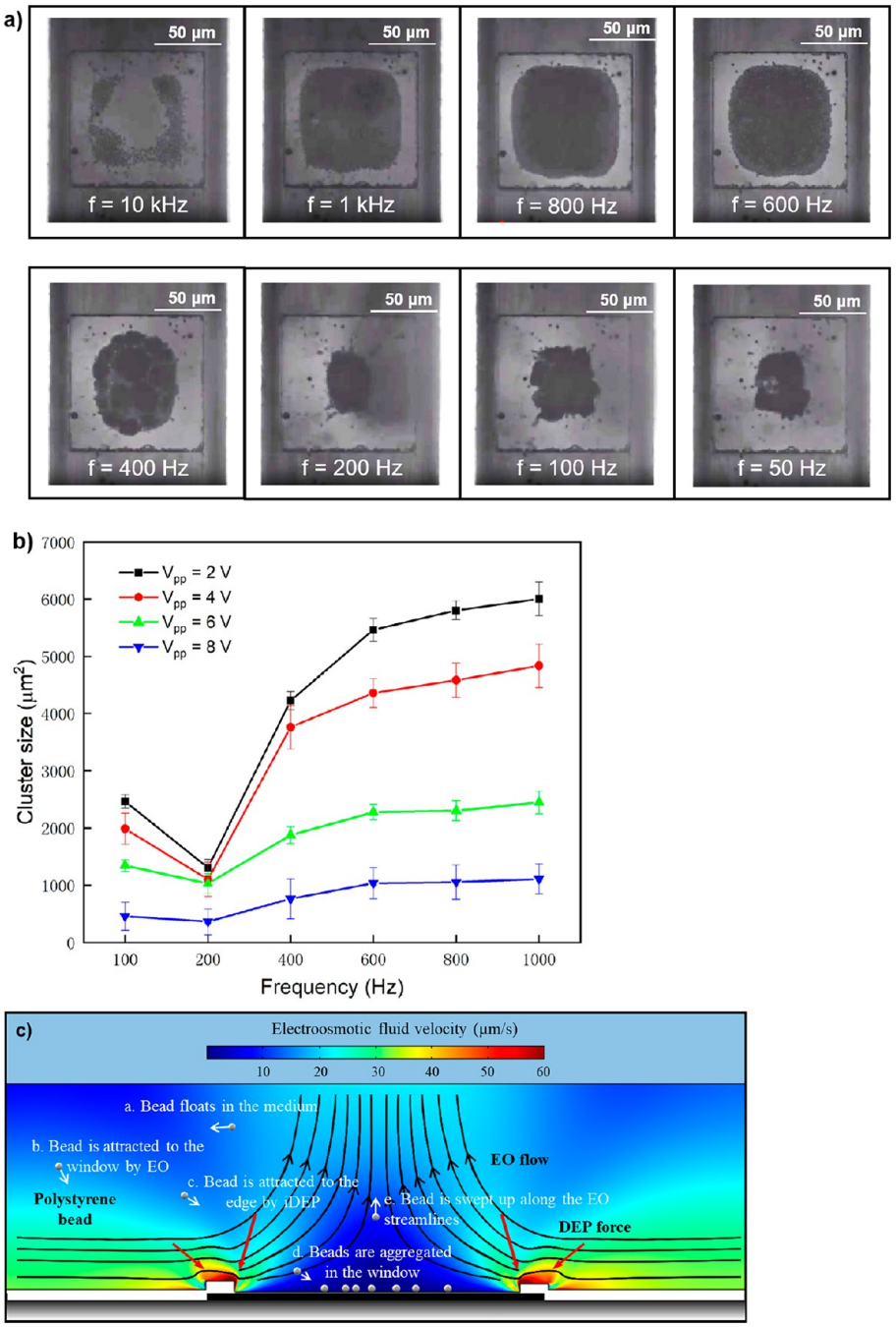

Figure 5. (a) 1 μm polystyrene beads are pushed together under the influence of electro-osmosis inside the wells at 3 Vpp as the applied frequency is decreased from 10 kHz to 50 Hz. (b) Frequency and voltage dependence of the 1 μm polystyrene bead clusters in 100 μm windows. (c) COMSOL model of EO streamlines around the resist window.

frequency and 4 Vpp (peak-to-peak). Under these conditions, the initially homogeneous suspension of 5 μm particles is forced into three areas: the trenches between the electrodes, the gaps between the wells, and the centers of the wells as seen in Figure 3a. Although this pattern was observed for all experiments with 5 μm beads during the described nDEP step, the 1 μm particle suspension under the same conditions remained homogeneously dispersed throughout the medium. The larger 5 μm beads gravitationally settle down to the level of the electrodes in a few minutes after the particle suspension is pipetted onto the electrodes (as discussed in detail in the Supporting Information). Once the beads are settled onto electrodes, the activation of the nDEP force repels the beads from the edges of the resist and pushes them in place within the wells of the electrodes and into other regions described above. In contrast, because the 1 μm beads remain suspended above the electrodes, nDEP force repels the beads away from the surface of the electrodes.

Once the nDEP step is performed, the frequency is lowered to 1 kHz, where the beads experience a positive DEP force. At this point, the 5 μm particles located in the trenches and gaps become attracted to the edges of the resist windows and are subsequently pulled into the centers of the wells, joining the cluster of particles as shown in Figure 2. Demonstration of this guided electrokinetic assembly process can be seen in the video

https://dx.doi.org/10.1021/acsami.0c08266
ACS Appl. Mater. Interfaces XXXX, XXX, XXX−XXX

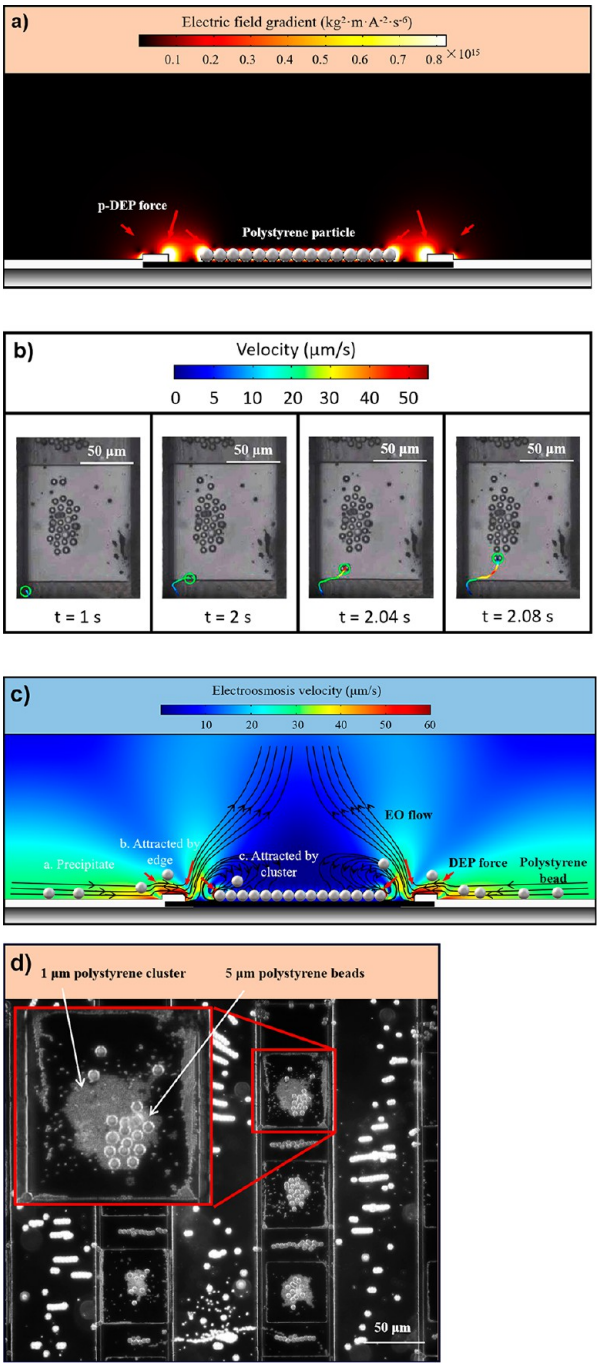

Figure 6. (a) COMSOL simulation result demonstrating two areas of high electric field gradients: around the edges of resist windows and around the particle cluster inside the window; (b) a series of optical micrographs tracing the movement of 5 μm bead toward the cluster of 5 μm beads inside the well under 1 kHz, 3 Vpp bias. (c) COMSOL model of EO streamlines around the resist window and cluster of the beads inside the window; (d) attraction of 5 μm particles by the cluster of 1 μm particles inside the wells.

clips in the Supporting Information. Furthermore, these clips offer comparison between the kinematics of the 1 and 5 μm beads under the influence of positive DEP. Here, one can observe that the 1 μm particles were propelled from the bulk of the medium toward the wells at velocities larger than those of the 5 μm beads. This difference in velocities is likely due to the smaller drag forces associated with the 1 μm beads as previously mentioned.

3.2. Movement of 5 μm Beads under DEP. The initial nDEP pattern formed by the 5 μm beads can be explained by the concentration of electric field lines near the edges of the photoresist windows in a process called insulator DEP (iDEP).[40] The strong negative DEP forces are produced around the photoresist edges that cover the electrodes. Some 5 μm beads will settle to the bottom of the electrode chip, including into the wells. Once nDEP is applied, the beads already located inside the wells will be pushed together into the center of each well away from the well sides, whereas beads located between the wells (on top of the resist) are also repelled away from the edges and form lines at the centers of these gaps. Similarly, within the bulk fluid surrounding the electrodes, the beads are pushed away from the resist-covered edges of the electrodes and form lines in the trenches between the electrodes as shown in Figure 3a. The influence of this nDEP force on the beads is demonstrated by the results of the COMSOL multiphysics simulation shown in Figure 3b.

Once the applied frequency is lowered to 1 kHz and the microbeads begin to experience a pDEP force, in addition to the edges of the resist, the clusters of microbeads inside the wells now also serve as points of highest electric field intensity. Under the influence of that pDEP force, remaining beads in the bulk of the fluid and in the gaps are attracted toward the wells. From the sequence of pictures shown in Figure 2, and in Video S1 and S2 for 5 μm beads, it can be seen that the positive iDEP forces near the edges of the wells begin attracting the particles previously positioned in the gaps between wells. Simultaneously, pearl chains in the trenches between the electrodes become attracted to the outer sides of the wells, where they eventually reposition themselves as demonstrated in the optical micrographs and multiphysics simulation results presented in Figure 4.

3.3. Movement of 1 μm Beads under the Influence of Electro-osmosis. For 1 μm beads, because of their small size, the DEP force is weak in comparison to the ACEO, and consequently, the beads act as tracers to reveal the nature of the ACEO flow. It has been demonstrated in the literature that electro-osmosis-driven vortices are induced at the edges of coplanar bar electrodes[30] as well as over the surface of the electrodes.[25] For the patterned electrodes, these EO vortices are generated above the wells at frequencies of 10 kHz and lower. Figure 5a demonstrates the interplay between the positive DEP force and ACEO flow and its corresponding frequency dependence that affects the size of the bead clusters inside the wells. In general with decreasing frequency, the vortices would expand from the edges of the wells toward their centers and push the beads inside the wells closer together. Figure 5b presents a plot that quantifies the area of the 1 μm polystyrene bead clusters as a function of the frequency and magnitude of the applied potential. As 1 μm beads are propelled toward the windows by EO flow, they pass over the outer resist edges and are positioned near the edge of the windows, where they experience a positive iDEP force. Although some of the microbeads become attracted to this edge, most of the beads are carried toward the exposed regions of the electrodes inside the windows. As the clusters of beads inside the windows continue to grow, the iDEP force near the clusters will also become increasingly larger. The velocity of the flow under the electrokinetic influence and the resulting movement of the microbeads was simulated in COMSOL and is presented in Figure 5c below.

https://dx.doi.org/10.1021/acsami.0c08266
ACS Appl. Mater. Interfaces XXXX, XXX, XXX−XXX

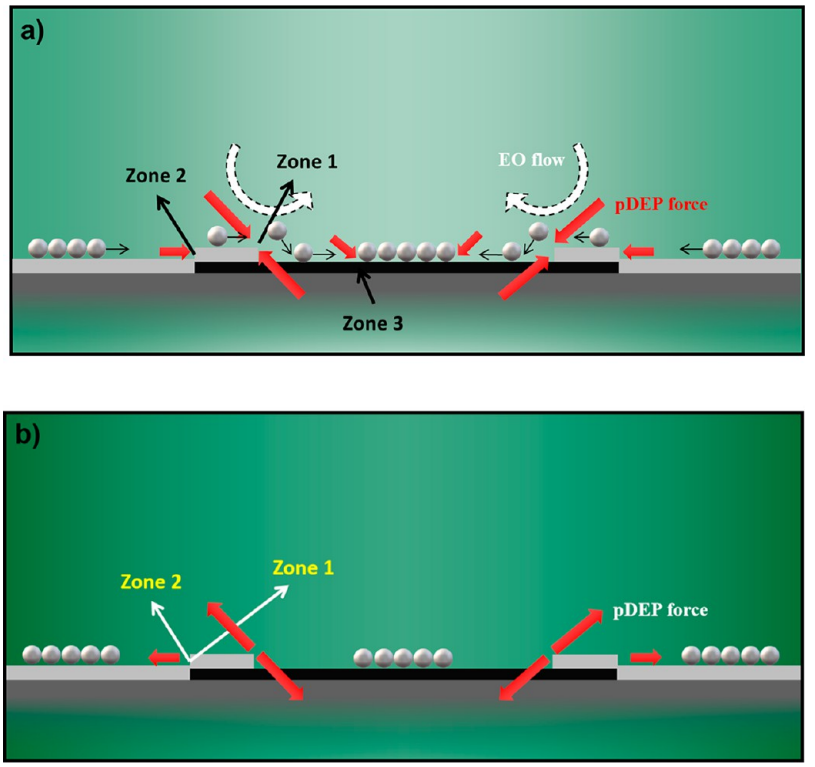

Figure 7. Mechanism of the guided electrokinetic assembly for 5 μm microparticles. The schematics represents a cross-section of the IDEA chip where the carbon electrodes are black, resist is gray, and the DEP forces are represented by red arrows and electro-osmotic forces by blue arrows. (a) Clustering of the 5 μm beads under the influence of n-DEP forces. (b) Schematics of the beads' motion under p-DEP forces and electro-osmotic (EO) forces that become significant under the low applied frequency. Zone 1 is the local maximum of iDEP forces at the inner edge of the resist well, Zone 2 is the local maximum of iDEP forces around the outer edge of the resist well, whereas Zone 3 is the local maximum for iDEP forces because of clustering of the polystyrene beads inside the wells.

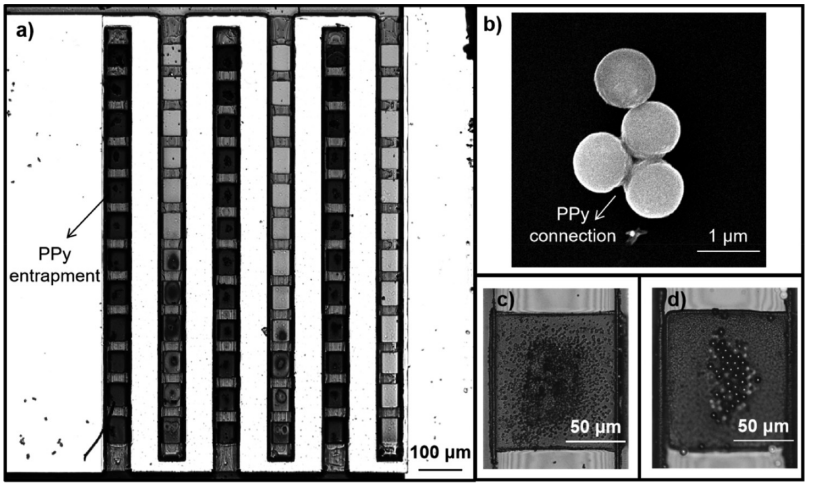

Figure 8. Entrapment of beads by PPy deposition. (a) Optical image of the IDEA with the polystyrene beads entrapped by PPy; (b) scanning electron microscopy (SEM) image of 1 μm bead agglomerate covered with PPy; (c) close-up of the well with PPy-entrapped 1 μm beads; (d) close-up of the well with PPy-entrapped 5 μm beads.

3.4. Template Electrokinetic Microassembly of 5 μm Beads inside Windows. As we discussed in section 3.3, at applied frequencies below 10 kHz, the 1 μm beads will fill the windows while under the influence of electro-osmosis. However, 5 μm beads under the same range of frequencies were observed to aggregate at the edges of the windows under the influence of the positive iDEP forces (see section 3.2) rather than in the windows because larger beads are more inertial and less influenced by the flow streamlines and more influenced by DEP forces that depend on the cube of particle radius (see eq 2 above). One strategy to facilitate the filling of windows by 5 μm beads is to allow some of the polystyrene beads to sediment inside the windows. These initial bead clusters inside the windows will later serve as areas of higher electric field intensity when the pDEP force is activated and will facilitate the assembly of the microbeads inside the windows. Figure 6a presents a COMSOL simulation of the iDEP forces for a cluster of polystyrene microbeads inside a window. Once the beads have

https://dx.doi.org/10.1021/acsami.0c08266
ACS Appl. Mater. Interfaces XXXX, XXX, XXX−XXX

been successfully localized in the wells, gaps, and trenches under the nDEP force, and once the pDEP force is activated, at this point, there is a competing pDEP influence between the cluster of the beads inside the window and the resist edge of the window (both regions serve as areas of high electric field intensity). Figure 6b demonstrates the observed movement of a 5 μm bead traveling from a gap toward a growing cluster of beads inside a well. The movement of the beads from the edge toward the centers of the wells is assisted by the electro-osmotic flow whose streamlines are simulated in Figure 6c.

Thus, to fill the windows in the resist with 5 μm beads, one can start with depositing of the bead suspension over the electrode array and waiting for several minutes for gravitational sedimentation to take place and then applying 1 MHz frequency to utilize negative DEP (see Figure 2). That initial step will ensure that some beads will already be inside the windows. Following that nDEP step with lowering frequency to 1 kHz to start positive DEP will result in filling the windows with 5 μm beads as seen in Figure 3a.

To avoid the need for gravitational sedimentation of the 5 μm beads, we explored an alternative strategy for attracting them to the windows. It was observed that when 1 μm beads were added to the 5 μm bead suspension, these smaller beads would begin filling the windows under the influence of ACEO at a frequency of 1 kHz (see section 3.3 above). The formation of 1 μm clusters then serve as areas of high electric field intensity, which subsequently allow for the successful attraction of 5 μm beads to the windows under positive DEP. Figure 6d illustrates this process of attracting 5 μm beads with the initial formation of 1 μm cluster using positive iDEP attraction.

Figure 7 summarizes the interplay of the DEP and EO forces for 5 μm beads in the template electrokinetic assembly (TEA) process.

3.5. Permanent Entrapment of the Beads with Polypyrrole. The permanent entrapment of 1 and 5 μm beads through polypyrrole electrodeposition is presented in Figure 8a–c. Because the PPy deposition is initiated by a DC offset, only one side of the electrode experiences PPy deposition. Deposition on the other side can still be achieved by switching the live and ground wires to reverse the polarity of the DC offset.

4. CONCLUSION

In this study, the guided electrokinetic microassembly of polystyrene microparticles onto specific locations of patterned carbon microelectrodes was presented. It was discovered that AC electro-osmosis under an applied frequency of 1 kHz is sufficient to effectively agglomerate 1 μm beads in the wells, whereas a stepwise process involving the application of a 1 MHz signal, followed by a 1 kHz signal, is required for the positioning of 5 μm beads, which are mainly affected by dielectrophoretic forces. The assembly sequence is divided into two steps: guided deposition of microparticles, followed by their permanent entrapment via electropolymerization of the conductive polymer, polypyrrole. Experimental evidence and numerical simulations presented in this study demonstrate the process of the guided assembly of microparticles under the combined influence of dielectrophoretic and electro-osmotic forces. It should be noted that the influence of secondary effects, such as natural convection were neglected in our analysis. The demonstrated guided electrokinetic assembly technique has the potential to be utilized in massively parallel microassembly processes for devices employed in a wide range of applications, from biotechnology to micro- and nanoelectronics. Furthermore, the microparts to be assembled may be made of a variety of materials, such as organic and inorganic matter, dielectric, and metallic materials. Our future work will focus on the reduction of the size of the windows opened in the resist and on using various nanoparticles. We will also conduct a study on the deposition and assembly of biological cells.

ASSOCIATED CONTENT

Supporting Information

The Supporting Information is available free of charge at https://pubs.acs.org/doi/10.1021/acsami.0c08266.

Movie S1, the template-based electrokinetically guided microassembly of 1 μm diameter polymer particles (MP4)

Movie S2, the template-based electrokinetically guided microassembly of 5 μm diameter polymer particles (MP4)

Gravitational sedimentation of 5 μm polystyrene particles and details of the experimental setup and temperature regime of the pyrolysis (PDF)

AUTHOR INFORMATION

Corresponding Author

Lawrence Kulinsky − *Department of Mechanical and Aerospace Engineering, University of California, Irvine, Irvine, California 92627, United States;* orcid.org/0000-0002-1176-3578; Email: lkulinsk@uci.edu

Authors

Tuo Zhou − *Department of Mechanical and Aerospace Engineering and Materials and Manufacturing Technology, University of California, Irvine, Irvine, California 92627, United States*

Jingyuan Chen − *Department of Materials Science and Engineering, Harbin Institute of Technology, Shenzhen, Shenzhen, Guangdong 518055, P.R. China*

Ethan Kropp − *Department of Mechanical and Aerospace Engineering, University of California, Irvine, Irvine, California 92627, United States*

Complete contact information is available at: https://pubs.acs.org/10.1021/acsami.0c08266

Author Contributions

The manuscript was written through contributions of all authors. All authors have given approval to the final version of the manuscript.

Notes

The authors declare no competing financial interest.

ACKNOWLEDGMENTS

The authors acknowledge the support of the National Science Foundation (award CMMI-1661877) and University of California, Irvine's Undergraduate Research Opportunity Program.

REFERENCES

(1) Razali, A. R.; Qin, Y. A Review on Micro-manufacturing, Micro-forming and their Key Issues. *Procedia Eng.* **2013**, *53*, 665−672.

(2) Cohn, M. B.; Boehringer, K. F.; Noworolski, J. M.; Singh, A.; Keller, C. G.; Goldberg, K. A.; Howe, R. T. Microassembly Technologies for MEMS. In *Microelectronic Structures and MEMS for*

Optical Processing IV; International Society for Optics and Photonics, 1998; Vol. *3512*, pp 2−16.
(3) Whitesides, G. M.; Grzybowski, B. Self-Assembly at All Scales. *Science* **2002**, *295*, 2418−2421.
(4) Grzelczak, M.; Vermant, J.; Furst, E. M.; Liz-Marzan, L. M. Directed Self-Assembly of Nanoparticles. *ACS Nano* **2010**, *4*, 3591−3605.
(5) Cecil, J.; Vasquez, D.; Powell, D. A Review of Gripping and Manipulation Techniques for Micro-assembly Applications. *Int. J. Prod. Res.* **2005**, *43*, 819−828.
(6) Yong Zhang; Chen, B.K.; Xinyu Liu; Yu Sun. Autonomous robotic pick-and-place of microobjects. *IEEE Transactions on Robotics* **2010**, *26*, 200−207.
(7) Gao, D.; Ding, W.; Nieto-Vesperinas, M.; Ding, X.; Rahman, M.; Zhang, T.; Lim, C.; Qiu, C. W. Optical Manipulation from the Microscale to the Nanoscale: Fundamentals, Advances and Prospects. *Light: Sci. Appl.* **2017**, *6*, e17039−e17054.
(8) Shimoyama, I. Scaling in Microrobots″ in *IEEE. Int. Conf. Intell. Robot. Syst* **1995**, *2*, 208−211.
(9) Fearing, R. S. Survey of Sticking Effects for Micro Parts Handling″ in *IEEE. Int. Conf. Intell. Robot. Syst* **1995**, *2*, 212−217.
(10) Keller, C. G.; Howe, R. T. Hexsil Tweezers for Teleoperated Micro-assembly″ in *Proc. IEEE the Tenth Annual Int. Workshop on Micro Electro Mech. Syst* **1997**, 72−77.
(11) Bhisitkul, R. B.; Keller, C. G. Development of Micro-electromechanical Systems (MEMS) Forceps for Intraocular Surgery. *Br. J. Ophthalmol.* **2005**, *89*, 1586−1588.
(12) Dechev, N.; Cleghorn, W. L.; Mills, J. K. Microassembly of 3-D Microstructures Using a Compliant, Passive Microgripper. *J. Microelectromech. Syst.* **2004**, *13*, 176−189.
(13) Perez-Gonzalez, V. H.; Ho, V.; Vazquez-Pinon, M.; Martinez-Chapa, S. O.; Kulinsky, L. A novel micro/nano fabrication process based on the combined use of dielectrophoresis, electro-osmotic flow, and electrodeposition for surface patterning. *J. Micromech. Microeng.* **2015**, *25*, 115007−115019.
(14) Barsotti, R. J., Jr; Vahey, M. D.; Wartena, R.; Chiang, Y. M.; Voldman, J.; Stellacci, F. Assembly of Metal Nanoparticles into Nanogaps. *Small* **2007**, *3*, 488−499.
(15) Buyong, M.; Kayani, A.; Hamzah, A.; Yeop Majlis, B. Dielectrophoresis Manipulation: Versatile Lateral and Vertical Mechanisms. *Biosensors* **2019**, *9*, 30−56.
(16) Fu, K.; Chen, S.; Zhao, J.; Willis, B. G. Dielectrophoretic Assembly of Gold Nanoparticles in Nanoscale Junctions for Rapid, Miniature Chemiresistor Vapor Sensors. *ACS Sensors* **2016**, *1*, 444−450.
(17) Xiong, X.; Busnaina, A.; Selvarasah, S.; Somu, S.; Wei, M.; Mead, J.; Chen, C. L.; Aceros, J.; Makaram, P.; Dokmeci, M. R. Directed Assembly of Gold Nanoparticle Nanowires and Networks for Nanodevices. *Appl. Phys. Lett.* **2007**, *91*, 063101−063103.
(18) Subramanian, A.; Vikramaditya, B.; Dong, L.; Bell, D.; Nelson, R. J. Micro and Nanorobotic Assembly Using Dielectrophoresis″ in *Int. Conf. on Robotics: Science and Syst* **2005**, *1*, 327−334.
(19) Velev, O. D.; Bhatt, K. H. On-chip Micromanipulation and Assembly of Colloidal Particles by Electric Fields. *Soft Matter* **2006**, *2*, 738−750.
(20) Kretschmer, R.; Fritzsche, W. Pearl Chain Formation of Nanoparticles in Microelectrode Gaps by Dielectrophoresis. *Langmuir* **2004**, *20*, 11797−11801.
(21) Vazquez-Pinon, M.; Pramanick, B.; Ortega-Gama, F. G.; Perez-Gonzalez, V. H.; Kulinsky, L.; Madou, M. J.; Hwang, H.; Martinez-Chapa, S. O. Hydrodynamic channeling as a controlled flow reversal mechanism for bidirectional AC electro-osmotic pumping using glassy carbon microelectrode arrays. *J. Micromech. Microeng.* **2019**, *29*, 075007−075021.
(22) Vázquez-Piñón, M.; Hwang, H.; Madou, M. J.; Kulinsky, L.; Martínez-Chapa, S. O. Comparison of Two-Dimensional and Three-Dimensional Carbon Electrode Geometries Affecting Bidirectional Electroosmotic Pumping. *Journal of Micro and Nano-Manufacturing* **2019**, *7*, 024510−024514.
(23) Cortez, J.; Damyar, K.; Gao, R.; Zhou, T.; Kulinsky, L. Electrokinetic Propulsion of Polymer Microparticulates Along Glassy Carbon Electrode Array. *Journal of Micro and Nano-Manufacturing* **2020**, *8*, 024504−024509.
(24) Zhou, T.; Kropp, E.; Chen, J.; Kulinsky, L. Step-Wise Deposition Process for Dielectrophoretic Formation of Conductive 50-Micron-Long Carbon Nanotube Bridges. *Micromachines* **2020**, *11*, 371−383.
(25) Ramos, A.; Morgan, H.; Green, N. G.; Castellanos, A. AC Electrokinetics: A Review of Forces in Microelectrode Structures. *J. Phys. D: Appl. Phys.* **1998**, *31*, 2338−2353.
(26) Sabouraud, G.; Sadki, S.; Brodie, N. The Mechanisms of Pyrrole Electropolymerization. *Chem. Soc. Rev.* **2000**, *29*, 283−293.
(27) Sayyah, S. M.; Abd El-Rehim, S. S.; El-Deeb, M. M. Electropolymerization of Pyrrole and Characterization of the Obtained Polymer Films. *J. Appl. Polym. Sci.* **2003**, *90*, 1783−1792.
(28) Li, C. M.; Sun, C. Q.; Chen, W.; Pan, L. Electrochemical Thin Film Deposition of Polypyrrole on Different Substrates. *Surf. Coat. Technol.* **2005**, *198*, 474−477.
(29) Squires, T. M.; Bazant, M. Z. Induced-Charge Electro-osmosis. *J. Fluid Mech.* **1999**, *509*, 217−252.
(30) Green, N. G.; Ramos, A.; González, A.; Morgan, H.; Castellanos, A. Fluid Flow Induced by Nonuniform AC Electric Fields in Electrolytes on Microelectrodes. III. Observation of Streamlines and Numerical Simulation. *Phys. Rev. E: Stat. Phys., Plasmas, Fluids, Relat. Interdiscip. Top.* **2002**, *66*, 026305−026315.
(31) González, A.; Ramos, A.; Green, N. G.; Castellanos, A.; Morgan, H. Fluid Flow Induced by Nonuniform AC Electric Fields in Electrolytes on Microelectrodes. II. A Linear Double-Layer Analysis. *Phys. Rev. E: Stat. Phys., Plasmas, Fluids, Relat. Interdiscip. Top.* **2000**, *61*, 4019−4028.
(32) Green, N. G.; Ramos, A.; González, A.; Morgan, H.; Castellanos, A. Fluid Flow Induced by Nonuniform AC Electric Fields in Electrolytes on Microelectrodes. I. Experimental Measurements. *Phys. Rev. E: Stat. Phys., Plasmas, Fluids, Relat. Interdiscip. Top.* **2000**, *61*, 4011−4018.
(33) Bruckenstein, S. Physicochemical Hydrodynamics. *Nature* **1977**, *268*, 298−299.
(34) Jones, T. B. *Electromechanics of Particles*; Cambridge University Press, 2005, pp 36−43.
(35) Ramos, A. *Electrokinetics and Electrohydrodynamics in Microsystems*; Springer Science & Business Media, 2011; Vol. *530*, pp 48−52.
(36) Pilot, R.; Signorini, R.; Durante, C.; Orian, L.; Bhamidipati, M.; Fabris, L. A Review on Surface-Enhanced Raman Scattering. *Biosensors* **2019**, *9*, 57−154.
(37) Lee, A. C.; Lee, Y.; Lee, D.; Kwon, S. Divide and Conquer: A Perspective on Biochips for Single-Cell and Rare-Molecule Analysis by Next-generation Sequencing. *APL Bioengineering* **2019**, *3*, 020901.
(38) Singh, A.; Jayaram, J.; Madou, M.; Akbar, S. Pyrolysis of Negative Photoresists to Fabricate Carbon Structures for Microelectromechanical Systems and Electrochemical Applications. *J. Electrochem. Soc.* **2002**, *149*, E78−E83.
(39) Stokes, G. G. On the Effect of Internal Friction of Fluids on the Motion of Pendulums. *Trans. Cambr. Philos.* **1851**, *9*, 1−86.
(40) Lapizco-Encinas, B. H.; Simmons, B. A.; Cummings, E. B.; Fintschenko, Y. Insulator-Based Dielectrophoresis for the Selective Concentration and Separation of Live Bacteria in Water. *Electrophoresis* **2004**, *25*, 1695−1704.

https://dx.doi.org/10.1021/acsami.0c08266
ACS Appl. Mater. Interfaces XXXX, XXX, XXX−XXX